Mathematical Model for Tapping Simulation to Predict Radial Pitch Diameter Difference of threads

Jie Ren (botao12330@hotmail.com)
Taiyuan University of Science and Technology
Xianguo Yan
Taiyuan University of Science and Technology

Original Research

Keywords:

Posted Date: February 12th, 2021

DOI: https://doi.org/10.21203/rs.3.rs-192937/v1

Noname manuscript No.
(will be inserted by the editor)

Mathematical model for tapping simulation to predict Radial Pitch Diameter Difference of threads

Jie Ren[1] · **Xianguo Yan**[1]

Received: date / Accepted: date

Abstract As the most important component of parts, thread has a great influence on the mechanical properties and service performance of parts. In order to ensure the quality of the thread, the thread quality inspection standard involves 11 main thread characteristics, of which the surface roughness of the thread is the most studied, and the research on Radial Pitch Diameter Difference (RPDD) is still blank. In this paper, a quasi-static model of the tapping process is developed based on the roundness error mechanism of the hole, which includes cutting force and cutting damping force. Due to the regenerative nature of cutting, the force on each cutting edge depends on both the tool's current position and previous position. According to the eigenvalues and eigenvectors of the discrete state-transition matrix, RPDD is finally determined, and the influence of the chamfer length and the spindle speed on RPDD is simulated by this model. The results demonstrate that the chamfer length and spindle speed will affect RPDD, and the RPDD is the smallest when the chamfer length is 2 threads and the spindle speed is 1400 rev/min. The development of this model not only provides a cheap and effective method for the study of RPDD, but also lays a foundation for further experimental research.

Keywords Mathematical model · Tapping · Radial Pitch Diameter Difference · Simulation

Jie Ren ·
Xianguo Yan(✉)
E-mail: botao12330@outlook.com
[1] School of Mechanical Engineering, Taiyuan University of Science and Technology

1 Introduction

In modern industry, threaded connections are often used when parts and pipe connections need to be assembled in a non-destructive manner. The performance of threaded connections is critical to many fields such as petroleum, aerospace, shipbuilding, high-speed rail, nuclear energy, and automobile manufacturing[1–3].According to statistics, threaded connections generally account for 60% of the total mechanical components in each machinery and equipment[4].Therefore, it is of great significance to improve thread processing quality[5].

Poor thread quality will affect the mechanical properties and service performance of the components, such as tensile strength, torsion strength, vibration resistance, connection reliability, pipeline tightness, etc.[2,3, 6].The factor that has the greatest influence on the mechanical properties and service performance of threaded components is the geometry and dimensional accuracy of the thread[2].Dong[2] and Leon[7] studied the influence of thread dimensional conformance on the self-loosening resistance and static strength of the threaded connection which will be greatly reduced due to the unqualified outer diameter, middle diameter or inner diameter of bolts and nuts. Nassar et al.[8] showed that unqualified thread root radius will adversely affect the fatigue performance of pre-tightened threaded fasteners. In order to ensure the quality of thread, the thread quality inspection standard involves 11 main thread characteristics, and RPDD is one of them. RPDD is defined as the maximum difference among the pitch diameters in all radial directions within a lead. When a thread with an excessive RPDD is matched with a qualified thread, the sharply changing contact area between the internal and external threads may cause uneven load distribution on the thread surface, and severe

stress concentration occurs at the position with a smaller pitch diameter, which accelerates wear and tear, shorten the service life, and severely cause "looseness" or even "slip buckle"[3].

Compared with external threads, it is more difficult to ensure the quality of internal threads, especially small diameter internal threads. The machining of internal threads is very complicated, which is usually the last process of workpiece manufacturing. Any machining failure or reduced accuracy can not achieve the perfect assembly of components without gaps, and even lead to huge economic losses[9, 10]. Tapping is a process widely used in the manufacturing of internal threads. Although in the past few years, other processing methods have been used to manufacture internal threads with great success, such as thread milling and turning[11–16], tapping is almost the only method to manufacture small diameter internal threads[17]. However, there are relatively few literatures on thread quality in tapping. Fromentin et al.[18] showed that the use of suitable oil-based lubricants in tapping can improve the mechanical properties and surface integrity of internal threads. Piska et al.[19] compared taps with PVD and TiN composite coatings and uncoated taps to process C45, and the results showed that the use of coatings can effectively reduce tool damage and improve the surface finish of threads. Hsu et al.[20] used the Taguchi method to test and analyze the influence of tool parameters and cutting conditions on thread quality during tapping, and found that the larger the helix angle, the worse the quality of the thread. Bratan et al.[21] developed a tool to improve the threading process considering the combined deforming-cutting tap. The results have shown that utilising proposed combined deforming-cutting taps in the processing of internal threads with a small diameter for M3-M6 in aluminium alloys enhanced the accuracy and surface quality of threads. It can be seen that the current literatures on the thread quality obtained by tapping is mostly focused on the influence of various factors on the thread surface quality, and the research on the RPDD of the thread is almost blank. Therefore, it is very necessary to analyze the factors that affect the dimensional of R-PDD by establishing a mathematical model of RPDD.

For a standard internal thread, its pitch diameter can be determined by the nominal diameter and pitch of the thread, that is, pitch diameter = nominal diameter-pitch × 0.6495.Therefore, it can be considered that R-PDD of the thread is the result of the combined effect of the roundness error of the root circle and the pitch error. The mechanism of roundness error of the root cycle is similar to that of the hole. From the literature[22], it is known that the roundness error of the hole is largely caused by the vibration of the drill. The tap usually shows transverse vibration, torsional vibration and axial vibration during tapping, but there is no coupling relationship between the transverse vibration and axial/torsional vibration of the tap[23]. Because the torsional stiffness and axial stiffness are much greater than the bending stiffness, the torsion and axial displacement of a cantilever tool (such as a tap) with a large length-to-diameter ratio is much smaller than the transverse displacement under a given force. Therefore, torsional vibration and axial vibration are ignored, that is, the pitch error generated in tapping is ignored. The pitch diameter of the thread is only related to the nominal diameter of the thread, which means that the R-PDD is caused by the roundness error of the root cycle. Bayly et al.[24] established a quasi-static reaming model to explain the vibration of the tool during the cutting process and the resulting roundness errors in reamed holes, and process parameters such as the direction and the angular frequency of rotation of the tool will affect the dimensional of the roundness error. Deng et al.[25] believed that the dynamic excitation force will cause the deflection and the vibration of the tool, leading the roundness error of the hole, and developed a system control equation composed of exciting force to study mechanism of roundness error of the hole. This will provide great help for this research.

Since the previous research in this area is still blank, the blind cutting experiments are not only difficult to determine the factors that affect the dimensional of R-PDD in tapping, but the cost of the experiment is also very high. Based on previous studies, this paper will establish a quasi-static model of vibration with reference to the analysis method of roundness error of the hole, and finally determine the dimensional of RPDD, laying a solid foundation for the next step of experimental research.

2 Quasi-static model

During the tapping process, as the tap enters the predrilled hole at an axial rate synchronized with the thread lead, each tooth cuts a layer of material from the surface formed by the previous tooth. In order to ensure the smooth execution of the cutting process, the thread end of the tap is made into a tapered surface with κ_r as a chamfer to truncated the full thread, and a number of straight flutes for chip evacuation evenly distributed over the entire thread length divide the thread into several continuously distributed cutting teeth. The major cutting edges of the chamfered section of the tap are formed by the intersection of the tapered surface and the straight flute surfaces, and the minor cutting

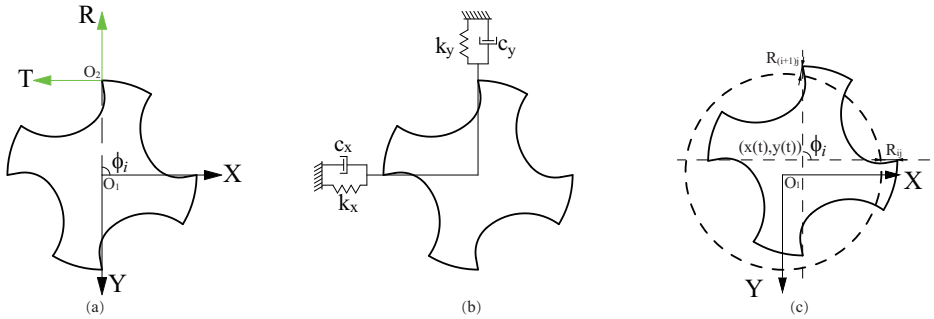

Fig. 1 Dynamic model of tapping process by considering the transverse vibrations

edges lie on the flank surfaces of the tap threads. As can be seen from the above description, the geometry of the tap is very complicated. In order to convenience the description of the tapping process, some coordinate systems first need to be established. The global coordinate system X-Y-Z whose origin O_1 is at the center of the hole is fixed on the workpiece surface, and the Z axis coincides with the hole axis. The cutting edge coordinate system is U-V-W with the origin O_2 at any designated point of the elementary cutting edge, and the W axis coincides with the major cutting edge. The local rotating coordinate system T-R-A is the transition coordinate system between the global coordinate system and the cutting edge coordinate system. Rotating the global coordinate system around the Z axis through ϕ_i can be converted into the T-R-A coordinate system that changes with the position of the elementary cutting edge, and then rotating this coordinate system around the X and Y axes through λ and κ_r respectively to convert to cutting edge coordinates system, as shown in Figures 1a and 2a. The three coordinate systems can be transformed into each other through the transformation matrix. The relationship between them can be expressed as:

$$\begin{bmatrix} X \\ Y \\ Z \end{bmatrix} = T_3 \begin{bmatrix} T \\ R \\ A \end{bmatrix} = T_1 T_2 T_3 \begin{bmatrix} U \\ V \\ W \end{bmatrix} \tag{1}$$

where

$$\begin{aligned} T_1 &= \begin{bmatrix} \cos\kappa_r & 0 & \sin\kappa_r \\ 0 & 1 & 0 \\ -\sin\kappa_r & 0 & \cos\kappa_r \end{bmatrix} \\ T_2 &= \begin{bmatrix} 1 & 0 & 1 \\ 0 & \cos\lambda & -\sin\lambda \\ 0 & \sin\lambda & \cos\lambda \end{bmatrix} \\ T_3 &= \begin{bmatrix} \cos\phi_i & -\sin\phi_i & 0 \\ \sin\phi_i & \cos\phi_i & 0 \\ 0 & 0 & 1 \end{bmatrix} \end{aligned} \tag{2}$$

As shown in Figure 1b, the dynamic model of the tap only considers the two orthogonal degrees of freedom of the tool in the radial direction. The differential equation of the two-degree-of-freedom transverse vibration of the dynamic tapping system in the global coordinate system is:

$$M\ddot{X} + C\dot{X} + KX = F \tag{3}$$

among them, M, C, K are the mass matrix, damping matrix and stiffness matrix of the tap respectively, and they are all second-order matrices.

Whitehead[26] and Towfighian[27] mentioned that the vibrations to cause roundness errors are divided into two categories: chatter and low frequency vibration. In tapping process, the speed of the tap is usually low, and the frequency is much lower than the lowest natural frequency of the tool. At this time, the stiffness term in the equation plays a leading role, while the inertia term and damping term can be ignored. Therefore the above equation becomes the following form:

$$KX = F \tag{4}$$

Equation 4 eliminated the inertia and damping terms in the transverse vibration differential equation is called a quasi-static model. The exciting force F includes regenerative cutting force and cutting damping force due to the waviness on the pre-drilled surface. For the convenience of research, let the number of tap flutes be N_f, and the tap are evenly dispersed into N_z slices with length dz along the axial direction, then the force of the entire tap is distributed to the $N_f \times N_z$ elementary cutting edges. According to the cutting principle of the tap, each elementary cutting edge is regarded as an oblique cutting model.

2.1 Cutting force

The cutting force of oblique cutting is proportional to the cross-sectional area of the chip to be removed. There-

fore, the cutting force F_c can be calculated by the following formula:

$$F_c = k_c A = k_c h b \tag{5}$$

where k_c is the cutting force coefficient, h is the cutting thickness, and b is the cutting width.

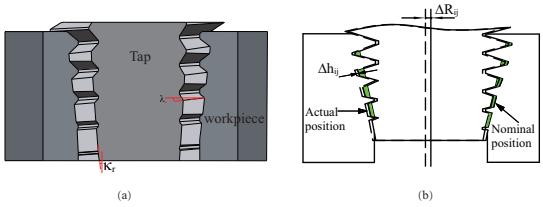

Fig. 2 Position change of the tap axis under transverse vibration

When the tool's actual trajectory (shown by the dashed line in Figure 2b) deviates from the nominal one due to transverse vibration (shown by the solid line in Figure 2b), an additional dynamic uncut chip thickness will attach to the desired static uncut chip thickness. Since the static uncut chip thickness does not cause vibration, only the load caused by the dynamic uncut chip thickness remains in the cutting force. Therefore, the radial, tangential and axial components of the cutting force of elementary cutting edge in the cutting edge coordinate system U-V-W can be expressed as:

$$\begin{bmatrix} \Delta F_{cu,ij} \\ \Delta F_{cv,ij} \\ \Delta F_{cw,ij} \end{bmatrix} = \begin{bmatrix} k_{cu} \\ k_{cv} \\ k_{cw} \end{bmatrix} \Delta h_{ij} dz \tag{6}$$

where Δh_{ij} represents the dynamic uncut chip thickness of the jth elementary cutting edge corresponding to the ith flute. If the transverse displacement of the tap axis at time t is represented by x(t) and y(t), the transverse displacement ΔR_{ij} of the elementary cutting edge can be determined by the displacement of the tap axis and the tooth angle ϕ_i(Figure 1c):

$$\Delta R_{ij} = R_{ij} - R_{(i-1)j} = \Delta x \cos\phi_i + \Delta y \sin\phi_i \tag{7}$$

where

$$\begin{aligned} \Delta x &= x(t) - x(t-\tau_0) \\ \Delta y &= y(t) - y(t-\tau_0) \end{aligned} \tag{8}$$

where τ_0 is the time interval between adjacent teeth. The dynamic uncut chip thickness can be expressed as:

$$\begin{aligned} \Delta h_{ij} &= \Delta R_{ij} \cos\kappa_r \\ &= [\Delta x \cos\phi_i + \Delta y \sin\phi_i] \cos\kappa_r \end{aligned} \tag{9}$$

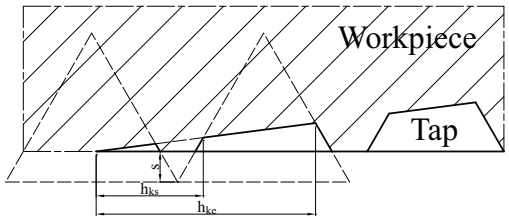

Fig. 3 Axial position of each cutting edge on the straight flute tap

As the tapping depth increases, each cutting edge will experience partial and full engagement status. Therefore, the cutting force is constantly changing with the effective cutting edge length involved in cutting during the continuous tapping process. It can be seen from the geometric relationship in Figure 3 that the length of the cutting edge can be determined by its start and end positions in the axial direction. The start and end positions of each cutting edge in the axial direction can be expressed as:

$$\begin{aligned} h_{ks} &= \frac{\sqrt{3}P(k - N_f)\cos\kappa_r}{2N_f \cos(\frac{\pi}{6} + \kappa_r)} \\ h_{ke} &= \frac{2sN_f \sin(2\kappa_r + \frac{\pi}{3})}{N_f(2\cos(2\kappa_r + \frac{\pi}{3}) - 1)} \\ &\quad - \frac{\sqrt{3}kP \sin 2\kappa_r + 2sN_f \cos(2\kappa_r + \frac{\pi}{6})}{N_f(2\cos(2\kappa_r + \frac{\pi}{3}) - 1)} \end{aligned} \tag{10}$$

where k represents the serial number of the cutting edge, h_{ks} is the start position of the kth cutting edge, h_{ke} is the end position of the kth cutting edge, and P is the pitch. Since the tap cutting edge is not continuously distributed, the window function g(z) is introduced to identify whether the elementary cutting edge corresponding to a certain flute engages with the workpiece at time t. The elementary cutting force can be expressed in the U-V-W coordinate system as:

$$\begin{aligned} &\begin{bmatrix} \Delta F_{cu,ij} \\ \Delta F_{cv,ij} \\ \Delta F_{cw,ij} \end{bmatrix} \\ &= \begin{bmatrix} k_{cu}\,[\Delta x \cos\phi_i + \Delta y \sin\phi_i]\cos\kappa_r \\ k_{cv}\,[\Delta x \cos\phi_i + \Delta y \sin\phi_i]\cos\kappa_r \\ k_{cw}\,[\Delta x \cos\phi_i + \Delta y \sin\phi_i]\cos\kappa_r \end{bmatrix} g(z) dz \end{aligned} \tag{11}$$

The elementary cutting force in the T-R-A coordinate system can be expressed as follows based on coordinate transformation:

$$\begin{bmatrix} \Delta F_{ct,ij} \\ \Delta F_{cr,ij} \\ \Delta F_{ca,ij} \end{bmatrix} = T_1 T_2 \begin{bmatrix} k_{cu}\left[\Delta x \cos\phi_i + \Delta y \sin\phi_i\right]\cos\kappa_r \\ k_{cv}\left[\Delta x \cos\phi_i + \Delta y \sin\phi_i\right]\cos\kappa_r \\ k_{cw}\left[\Delta x \cos\phi_i + \Delta y \sin\phi_i\right]\cos\kappa_r \end{bmatrix} g(z)dz \tag{12}$$

where

$$g(z) = \begin{cases} 1, z \in (h_{ks}, h_{ke}), k = 0, 1, 2, ... \\ 0, others \end{cases} \tag{13}$$

$$\begin{aligned} k_{cu} &= \frac{\tau_s}{\sin\psi_n} \frac{\cos(\beta_n - \gamma_n) + \tan\lambda \tan\eta \sin\beta_n}{\sqrt{\cos^2(\psi_n + \beta_n - \gamma_n) + \tan^2\eta \sin^2\beta_n}} \\ k_{cv} &= \frac{\tau_s}{\sin\psi_n \cos\lambda} \frac{\sin(\beta_n - \gamma_n)}{\sqrt{\cos^2(\psi_n + \beta_n - \gamma_n) + \tan^2\eta \sin^2\beta_n}} \\ k_{cw} &= \frac{\tau_s}{\sin\psi_n} \frac{\cos(\beta_n - \gamma_n)\tan\lambda + \tan\eta \sin\beta_n}{\sqrt{\cos^2(\psi_n + \beta_n - \gamma_n) + \tan^2\eta \sin^2\beta_n}} \end{aligned} \tag{14}$$

where τ_s is the shear stress, ψ_n is the normal shear angle, λ is the inclination angle, β_n is the normal friction angle, γ_n is the normal rake angle, and η is the chip flow angle, and these values can be obtained according to the method in literature [28,29].In the T-R-A coordinate system, the cutting force of all elementary cutting edges corresponding to a certain flute can be expressed as:

$$\begin{bmatrix} \Delta F_{ct,i} \\ \Delta F_{cr,i} \\ \Delta F_{ca,i} \end{bmatrix} = \int_l^{l_0} T_1 T_2 \begin{bmatrix} k_{cu} \\ k_{cv} \\ k_{cw} \end{bmatrix} \left[\cos\phi_i \ \sin\phi_i\right] \cos\kappa_r g(z)dz \begin{bmatrix} \Delta x \\ \Delta y \end{bmatrix} \tag{15}$$

where l_0 is the start cutting position, l is the current cutting position, they can be expressed as:

$$\begin{aligned} l_0 &= \frac{D_h - d_0}{2\tan\kappa_r} \\ l &= \frac{nPt}{2\pi} \end{aligned} \tag{16}$$

where D_h is the diameter of the pre-drilled hole with a value of 8.5mm, d is the tap nominal diameter, and d_0 is the chamfer point diameter.

$$d_0 = d - 1.2P \tag{17}$$

By converting the cutting forces of all flutes from the local coordinate system to the global coordinate system and then adding them, the cutting forces ΔF_{cx}, ΔF_{cy} and ΔF_{cz} in the tangential, radial and axial directions of the tap can be calculated as follows:

$$\begin{bmatrix} \Delta F_{cx} \\ \Delta F_{cy} \\ \Delta F_{cz} \end{bmatrix} = \sum_i^{N_f} T_3 \int_l^{l_0} T_1 T_2 \begin{bmatrix} k_{cu} \\ k_{cv} \\ k_{cw} \end{bmatrix} \left[\cos\phi_i \ \sin\phi_i\right] \cos\kappa_r g(z)dz \begin{bmatrix} \Delta x \\ \Delta y \end{bmatrix} \tag{18}$$

through simplification, Equation 18 can be expressed as:

$$\begin{bmatrix} \Delta F_{cx} \\ \Delta F_{cy} \end{bmatrix} = K_c \begin{bmatrix} \Delta x \\ \Delta y \end{bmatrix} \tag{19}$$

where

$$K_c = \sum_i^{N_f} T_3 \int_l^{l_0} T_1 T_2 \begin{bmatrix} k_{cu} \\ k_{cv} \\ k_{cw} \end{bmatrix} \left[\cos\phi_i \ \sin\phi_i\right] \cos\kappa_r g(z)dz \tag{20}$$

2.2 Cutting damping force

The actual cutting edge is not sharp, but is a small arc, as shown in Figure 4b.Therefore, the edge force and the cutting damping force are generated because the material under the flank face of the cutting edge is extruded[30].Since the edge force does not cause vibration, only the cutting damping force remains. The cutting damping force is caused by the interference between the uneven workpiece surface caused by the tool vibration and the tool flank surface, which causes the effective flank angle α_{eff} (as shown in Figure 4a) to change. Literature [31] mentioned that the cutting damping force is composed of the normal force F_{dv} and the friction force F_{du}, and the normal force F_{dv} is proportional to the volume V of the workpiece material extruded under the flank face of the cutting edge:

$$F_{dv} = K_{sp} V \tag{21}$$

where K_{sp} is the specific contact force, which depends on the material and the geometry of the cutting edge. The volume V is related to the geometry of the cutting edge, the vibration speed $\dot{c}$ perpendicular to the machined surface and the cutting speed v_c (Figure 4a):

$$V = \frac{1}{2} l_w^2 \frac{\dot{c}}{v_c} b \tag{22}$$

where l_w is the interference length between the workpiece surface and the flank face of the tool. According to the model proposed by Ahmadi et al.[30], the interference length l_w can be written as:

$$l_w = l_h + l_c + l_f \tag{23}$$

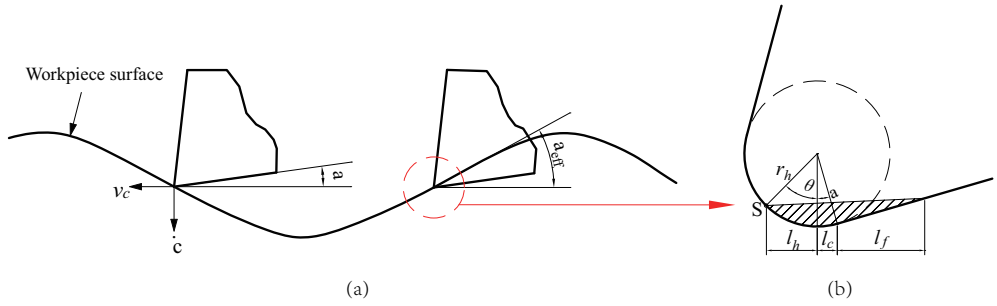

Fig. 4 Tool path and cutting damping force geometry

where

$$\begin{aligned} l_h &= r_h \sin\theta \\ l_c &= r_h \sin\alpha \\ l_f &= r_h[\cos\alpha - \cos\alpha]\cot\alpha \end{aligned} \tag{24}$$

where r_h is the hone radius, α is the flank angle and θ is the separation angle which defines the position where the workpiece material is no longer removed as chips through the rake face, but is extruded under the flank face of the tool. Therefore, the normal component F_{dv} of the cutting damping force can be written as:

$$F_{dv} = k_v \frac{\dot{c}}{v_c} b \tag{25}$$

where

$$k_v = \frac{1}{2} K_{sp} l_w^2 \tag{26}$$

The friction component F_{du} of the cutting damping force is considered to be proportional to the normal component F_{dv}, so it can be written as:

$$F_{du} = \mu F_{dv} \tag{27}$$

where μ is the Coulomb friction coefficient, which is taken as 0.3 according to literature [32]. Therefore, the radial and tangential components of the cutting damping force of the elementary cutting edge in the U-V-W coordinate system can be expressed as:

$$\begin{bmatrix} \Delta F_{du,ij} \\ \Delta F_{dv,ij} \\ \Delta F_{dw,ij} \end{bmatrix} = \begin{bmatrix} \mu k_v \\ k_v \\ 0 \end{bmatrix} \frac{\Delta h_{ij}}{\tau v_c} dz \tag{28}$$

where n is the spindle speed, v_c is the cutting speed at different axial positions.

$$v_c = [\pi d_0 + nPt \tan\kappa_r] n \tag{29}$$

Substituting the dynamic uncut chip thickness into Equation 28, and then based on the coordinate transformation, the elementary cutting damping force in the T-R-A coordinate system can be determined as follows:

$$\begin{aligned} &\begin{bmatrix} \Delta F_{dt,ij} \\ \Delta F_{dr,ij} \\ \Delta F_{da,ij} \end{bmatrix} \\ &= T_1 T_2 \begin{bmatrix} \frac{\mu k_v [\Delta x \cos\phi_i + \Delta y \sin\phi_i] \cos\kappa_r}{\tau v_c} \\ \frac{k_v [\Delta x \cos\phi_i + \Delta y \sin\phi_i] \cos\kappa_r}{\tau v_c} \\ 0 \end{bmatrix} g(z) dz \end{aligned} \tag{30}$$

Like the method of obtaining the cutting force, the tangential ΔF_{dx}, radial ΔF_{dy} and axial ΔF_{dz} components of the cutting damping force can be expressed as:

$$\begin{aligned} &\begin{bmatrix} \Delta F_{dx} \\ \Delta F_{dy} \\ \Delta F_{dz} \end{bmatrix} \\ &= \sum_i^{N_f} T_3 \int_l^{l_0} T_1 T_2 \begin{bmatrix} \frac{\mu k_v}{\tau v_c} \\ \frac{k_v}{\tau v_c} \\ 0 \end{bmatrix} [\cos\phi_i \ \sin\phi_i] \cos\kappa_r g(z) dz \begin{bmatrix} \Delta x \\ \Delta y \end{bmatrix} \end{aligned} \tag{31}$$

through simplification, Equation 31 can be expressed as:

$$\begin{bmatrix} \Delta F_{dx} \\ \Delta F_{dy} \end{bmatrix} = K_v \begin{bmatrix} \Delta x \\ \Delta y \end{bmatrix} \tag{32}$$

where

$$\begin{aligned} &K_v = \\ &\sum_i^{N_f} T_3 \int_l^{l_0} T_1 T_2 \begin{bmatrix} \frac{\mu k_v}{\tau v_c} \\ \frac{k_v}{\tau v_c} \\ 0 \end{bmatrix} [\cos\phi_i \ \sin\phi_i] \cos\kappa_r g(z) dz \end{aligned} \tag{33}$$

2.3 Elastic force

In the quasi-static equation, KX is the elastic force, where K is the stiffness matrix of the tool. For a two-degree-of-freedom system, it can be expressed as:

$$K = \begin{bmatrix} k_{xx} & k_{xy} \\ k_{yx} & k_{yy} \end{bmatrix} \tag{34}$$

Due to the small bending deformation of the tool, the vibration of the tool can be considered to be restricted to a plane perpendicular to the axis of the undeflected tool. Therefore, the relationship between the elastic force and the axis offset can be expressed as:

$$KX = \begin{bmatrix} k_{xx} & k_{xy} \\ k_{yx} & k_{yy} \end{bmatrix} \begin{bmatrix} x(t) \\ y(t) \end{bmatrix} \tag{35}$$

It is assumed that the tap is a cantilever beam whose force is concentrated on the tip of the tool in this analysis. According to literature [27],the stiffness matrix can be written as:

$$K = \frac{EI}{L^3} \begin{bmatrix} 3 & 0 \\ 0 & 3 \end{bmatrix} \tag{36}$$

where EI is the bending stiffness of the tool material,E is the elastic modulus of material of the tap,and L is the total length of the tap.

2.4 Solutions of quasi-static equations

Now substituting Equations 19 and 32 into Equation 4, the quasi-static equilibrium equation is rewritten as follows according to the displacement of the tap axis:

$$KX = K_c[X - X(t - \tau_0)] + K_v[X - X(t - \tau)] \tag{37}$$

The current value of X is expressed as a function of the previous value, and the friction time delay τ is approximately a fraction of the cutting time delay τ_0, that is, $\tau = \tau_0/m$. Therefore, the successive tool axis position equation can be expressed as:

$$X = A(t - \tau)X(t - m\tau) + B(t - \tau)X(t - \tau) \tag{38}$$

where

$$\begin{aligned} A(t) &= [K - K_c(t) - K_v(t)]^{-1} K_c(t) \\ B(t) &= [K - K_c(t) - K_v(t)]^{-1} K_v(t) \end{aligned} \tag{39}$$

Equation 38 is a difference equation with variable coefficients. In order to obtain the solution of the equation, based on the freezing coefficient method[33], the successive cutting process is discretized into several steps with time τ, each of which is approximated by a constant coefficient difference equation. For the convenience of solving, Equation 38 is written as a large matrix form:

$$\begin{aligned} &\begin{bmatrix} X(t) \\ X(t-\tau) \\ \vdots \\ X(t - m\tau + \tau) \end{bmatrix} \\ &= \begin{bmatrix} B(t-\tau) & 0 & \cdots & 0 & A(t-\tau) \\ I & 0 & \cdots & \cdots & 0 \\ \vdots & \ddots & \ddots & & \vdots \\ \vdots & & \ddots & \ddots & \vdots \\ 0 & \cdots & \cdots & I & 0 \end{bmatrix} \times \begin{bmatrix} X(t-\tau) \\ X(t-2\tau) \\ \vdots \\ X(t-m\tau) \end{bmatrix} \end{aligned} \tag{40}$$

this is

$$q_t = Q_{t-\tau} q_{t-\tau} \tag{41}$$

where the matrix $Q_{t-\tau}$ is the state-transition matrix at time $t-\tau$,I is a second-order identity matrix. According to the literature [34], Equation 41 can be written as follows:

$$Q_{t-\tau} q_{t-\tau} = \mu_{t-\tau} q_{t-\tau} \tag{42}$$

where

$$\mu = e^{\lambda\tau} \tag{43}$$

where λ is a characteristic exponent, whose imaginary and real parts represent the oscillation frequency and growth or decay rate respectively.

Equation 42 is a characteristic equation with m eigenvalues. The eigenvalues and eigenvectors satisfying the matrix $Q_{t-\tau}$ are $\mu_{t-\tau}$ and $q_{t-\tau}$ respectively, which can be determined by solving the characteristic equation. Therefore, the instantaneous position vector ${X^i}_{t-\tau}$ of m modes at time $t - \tau$ can be extracted from the m eigenvectors respectively. The displacement vector X^i of the ith mode at time t can be written as:

$$X^i = \mu^i_{t-\tau} X^i_{t-\tau}, (i = 1, 2, ..., m) \tag{44}$$

At time t, the displacement vector X of the tool axis can be obtained by superimposing the displacement vectors of m modes. The pitch diameter of the thread will also change with the axis offset. The pitch diameter at time t can be expressed as:

$$D_2(t) = \Delta D(t) + D - 0.6495P \tag{45}$$

where $D_2(t)$ is the pitch diameter of the thread at time t, and D is the nominal diameter of the thread which is equal to the nominal diameter d of the tap,the offset $\Delta D(t)$ at time t can be expressed as:

$$\Delta D(t) = x(t)\cos\phi(t) + y(t)\sin\phi(t) \tag{46}$$

where $\phi(t)$ is the angle of rotation in time t.

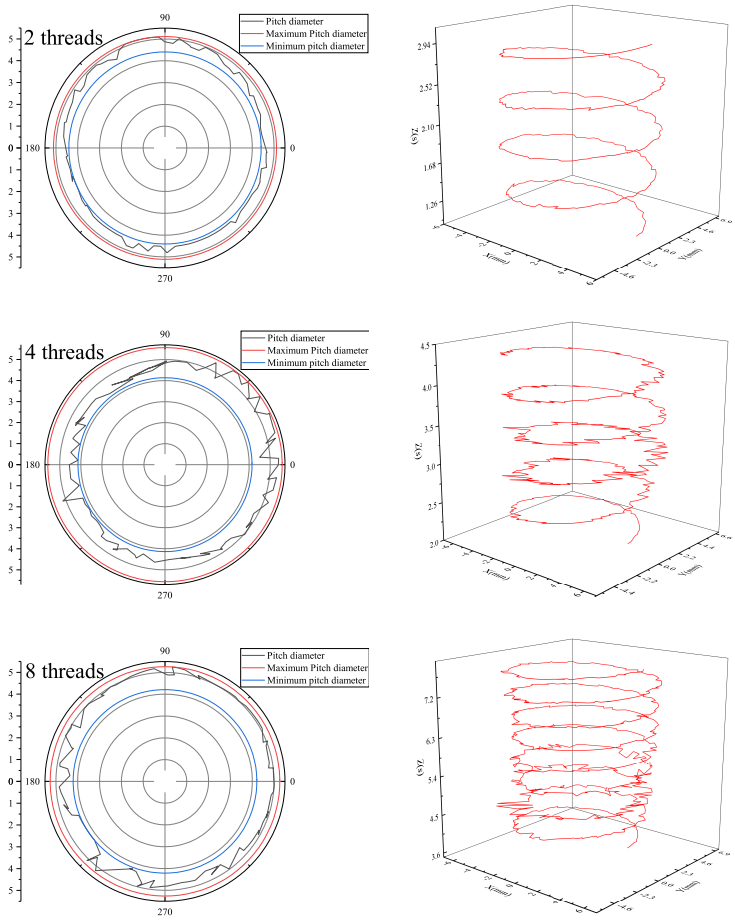

Fig. 5 Change of the pitch diameter of the first full thread and the movement trajectory of the outermost cutting edge of the tap in the global coordinate system during the entire cutting process when the chamfer length is 2 threads, 4 threads and 8 threads

Table 1 Geometric parameters of straight flute taps

Nominal Diameter (mm)	Tap Length (mm)	Rake Angle (deg)	Flank Angle (deg)	Flute Number
10	80	8	4	3

Table 2 Parameters of each group test

	1	2	3	4	5	6
Spindle Speed (rev/min)	700	1050	1400	1750	700	700
Chamfer Length (threads)	4	4	4	4	2	8

RPDD of the thread can be expressed as the difference between the maximum and minimum pitch diameters:

$$RPDD = D_{2max} - D_{2min} \tag{47}$$

where D_{2max} and D_{2min} are the maximum and minimum pitch diameters of the thread, respectively.

3 Simulation

Time domain simulation is performed based on the tool motion equation of Equation 38, which is also quasi-static. The static equilibrium position of the tool, subject to regenerative cutting and cutting damping forces, is found at every time step in the simulation, and then the dimensional of RPDD is determined by the Equation 47.The tool used in the simulation is a standard straight flute high-speed steel tap, and its parameters are shown in Table 1.The workpiece is an AISI1045 plate with pre-drilled holes. In the cutting simulation, 6 groups of tests whose parameters are listed in Table 2 were performed to study the influence of the chamfer length and the spindle speed on RPDD.

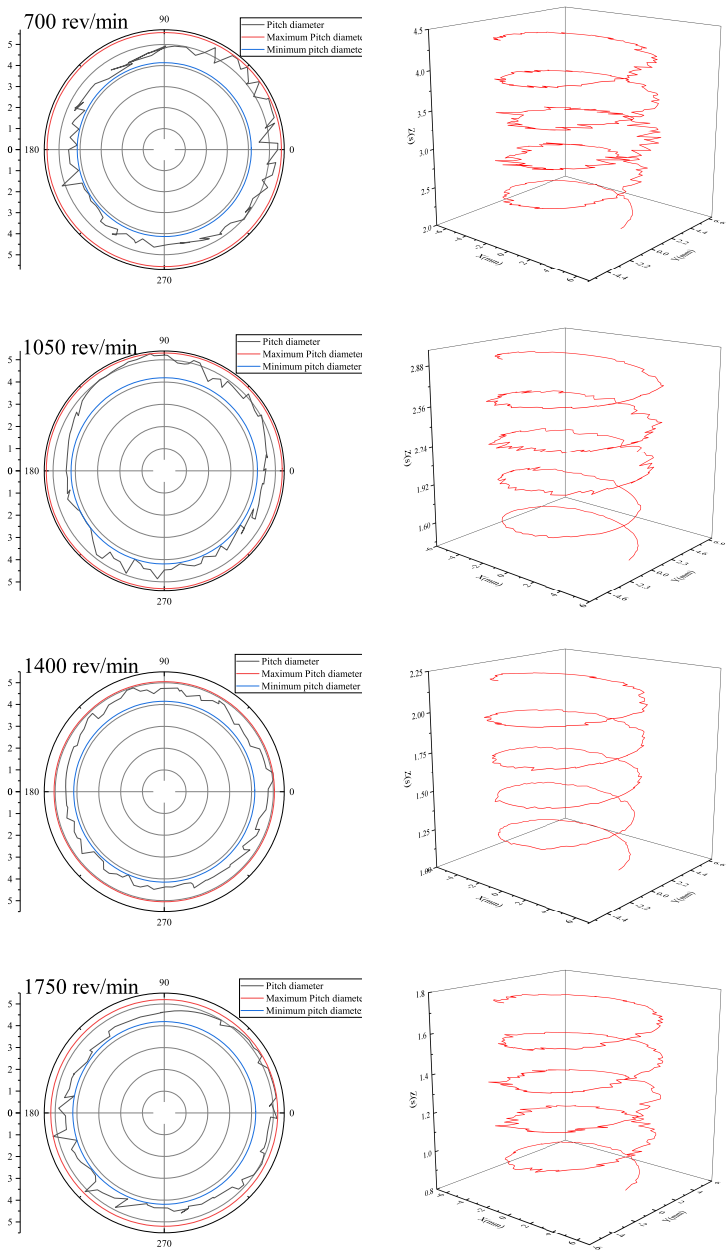

Fig. 6 Change of the pitch diameter of the first full thread and the movement trajectory of the outermost cutting edge of the tap in the global coordinate system during the entire cutting process when the spindle speed is 700rev/min, 1050rev/min, 1400rev/min and 1750rev/min

4 Results

From the simulation results, it is found that the imaginary part of the characteristic exponent of each mode remains almost unchanged over time, while the real part starts from a negative value and gradually becomes positive as time passes and the tap proceeds, resulting in an increase in the vibration amplitude. With the further engagement of the cutting edge and the workpiece, the real part will decrease and eventually remain constant, and the tool begins to vibrate periodically. The change of chamfer length and spindle speed will affect the characteristic exponent. As the chamfer length increases, the increase in the real part of the characteristic exponent will increase, while the increase in the spindle speed will reduce the rate of change of the real part of the characteristic exponent.

In order to analyze the influence of the chamfer length and the spindle speed on RPDD, the eigenvalues and eigenvectors of all modes of each group of tests are obtained by simulation. The vibrations of first four modes which are selected from all modes according to the rate of decay or growth of each mode because of their importance are considered here, and RPDD obtained is a combination of these four modes.

Figure 5 shows the change of the pitch diameter of the first full thread and the movement trajectory of the outermost cutting edge of the tap in the global coordinate system during the entire cutting process when the chamfer length is 2 threads, 4 threads and 8 threads. From the comparison of the three figures, it is found that the change of the chamfer length has an effect on RPDD.As can be seen in Figure 7a, the dimensional of RPDD shows a trend of first increasing and then decreasing with the increase of the chamfer length and the smallest RPDD is obtained when the chamfer length is 2 threads. The possible reason is that fewer cutting edges are involved in cutting, causing the vibration amplitude to increase briefly and then become a steady periodic vibration.

Figure 6 shows the change of the pitch diameter of the first full thread and the movement trajectory of the outermost cutting edge of the tap in the global coordinate system during the entire cutting process when the spindle speed is 700 rev/min, 1050 rev/min, 1400 rev/min and 1750 rev/min. From the comparison of the three figures, it is found that the change of the spindle speed has an effect on RPDD.As can be seen in Figure 7b, the dimensional of RPDD shows a trend of first decreasing and then increasing with the increase of the spindle speed and the smallest RPDD is obtained when the chamfer length is 1400 rev/min. The possible reason is that more cutting edges quickly participate in cutting when the spindle speed increases, resulting in a rapid increase in damping and a decrease in amplitude. But at the same time, the increase of the spindle speed will also lead to the decrease of the damping change rate, so a higher speed will restrain the amplitude reduction.

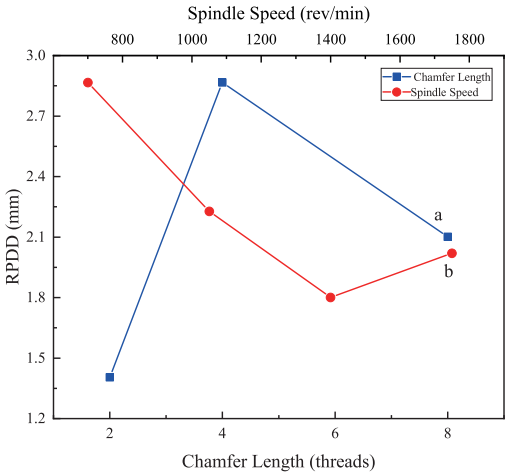

Fig. 7 Dimensional of RPDD under different spindle speed and chamfer length

5 Summary

A quasi-static tapping model, including delayed cutting force and cutting damping force was established. A similar cutting force model and cutting damping force were developed based on the work of previous researchers. The force equilibrium equation is expressed as a discrete-time matrix equation describing the successive state of the tool. According to the eigenvalues and eigenvectors of the state transition matrix, the characteristic solution of the equilibrium equation is found, and then RPDD is predicted from the characteristic solutions of the first four modes.

This model was used to simulate the tapping of AISI1045 plates using standard straight flute high-speed steel taps, and the dimensional of RPDD under different chamfer lengths and spindle speeds was obtained. By comparison, it is found that the chamfer length and spindle speed will affect RPDD, and RPDD is the smallest when the chamfer length is 2 threads and the spindle speed is 1400 rev/min. Since the research on RPDD is still blank so far, the development of this model not only provides a cheap and effective method for the study of RPDD, but also lays a foundation for further experimental research.

This model provides a method for the research of RPDD and the research on the stability of tapping in the literature [23] also confirms the conclusion of this article, but it needs to be verified by experiments in order to better illustrate its effectiveness. In addition, in the actual tapping process, the distributed force acts on the entire engagement length of the tool, but this model applies concentrated force on the tip of the tool, which will have a certain impact on the accuracy of the model. These issues will be studied in the future.

Funding information The research is financially supported by the National Natural Science Foundation of China (No. 51275333)

Conflict of interest

The authors have no relevant financial or non-financial interests to disclose.

Availability of data and material

The data sets supporting the results of this article are included within the article and its additional files.

Authors' contributions

Jie Ren developed a mathematical model to predict the radial diameter difference of threads, analyzed the simulation results, and was a major contributor in writing the manuscript. Xianguo Yan provided guidance for the writing of manuscript. All the authors read and approved the final manuscript.

Ethics approval

All analyses in this paper are based on previously published research and this paper does not involve animal and human testing, so this item is not applicable to this paper.

Consent to participate

All analyses in this paper are based on previously published research and this paper does not involve animal and human testing, so this item is not applicable to this paper.

Consent for publication

The Author confirms:
that the work described has not been published before (except in the form of an abstract or as part of a published lecture, review or thesis);
that it is not under consideration for publication elsewhere;
that its publication has been approved by all co-authors ,if any;
that its publication has been approved (tacitly or explicitly) by the responsible authorities at the institution where the work is carried out.
The author agrees to publication in the Journal indicated below and also to publication of the article in English by Springer in Springer's corresponding English-language journal. The copyright of the English article is transferred to Springer effective if and when the article is accepted for publication.

References

1. Fetullazade E, Akyildiz HK, Saritas S (2010) Effects of the machining conditions on the strain hardening and the residual stresses at the roots of screw threads. Mater Des 31:2025-2031.
2. Dong Y, Hess DP (1999) The effect of thread dimensional conformance on vibration-induced loosening. J Vib Acoust 121:209–213.
3. Korin I, J. Perez Ipina (2011) Experimental evaluation of fatigue life and fatigue crack growth in a tension bolt–nut threaded connection. Int J Fatigue 33:166-175.
4. Pesin MV (2012) Improving the reliability of threaded pipe joints. Russ Eng Res 32:210–212.
5. Min J (2015) Comprehensive measurement system for screw thread parameter based on machine vision. In: 2015 International Conference on Computer and Computational Sciences (ICCCS), pp 266-270
6. Araujo AC, Mello GM, Cardoso FG (2015) Thread milling as a manufacturing process for API threaded connection: Geometrical and cutting force analysis. J Manuf Process 18:75-83.
7. F.M Leon and N.G Pai and D.P Hess (2001) The effect of thread dimensional conformance on yield and tensile strength. Eng Fail Anal 8:49-56.
8. Nassar SA, Munn BS, Yang X (2009) Effect of Non-Conforming Thread Root Radius on the Fatigue Performance of Preloaded Threaded Fasteners. In: ASME 2008 Pressure Vessels and Piping Conference, pp 803-809.
9. Carvalho AOD, Brandão LC, Panzera TH, Lauro CH (2012) Analysis of form threads using fluteless taps in cast magnesium alloy (AM60). J Mater Process Technol 212:1753-1760.
10. Igor, Cézar, Pereira, et al (2016) Analysis of tapping process in three types of cast iron. Int J Adv Manuf Technol 82:1041-1048.
11. Malkov OV, Malkova LD (2019) Improving thread accuracy in machining components for rocket and space technologies. AIP Conf Proc 2171:200006.
12. Khoshdarregi M, Altintas Y (2018) Dynamics of multi-point thread turning—part I: General formulation. J Manuf Sci Eng 140: 061003.
13. Araujo AC, Fromentin G (2018) Investigation of tool deflection during milling of thread in Cr-Co dental implant. Int J Adv Manuf Technol 99, 531-541.
14. Malkov OV, Karelsky AC (2019) Rising the work uniformity of thread milling cutters in machining parts of rocket and space technology. AIP Conf Proc 2171:200005.
15. Wan M, Altintas Y (2014) Mechanics and dynamics of thread milling process. Int J Mach Tools Manuf 87:16-26.
16. Khoshdarregi MR, Altintas Y (2015) Generalized modeling of chip geometry and cutting forces in multi-point thread turning. Int J Mach Tools Manuf 98:21-32.
17. Wan M, Ma YC, Feng J, Zhang WH (2017) Mechanics of tapping process with emphasis on measurement of feed error and estimation of its induced indentation forces. Int J Mach Tools Manuf 114:8-20.
18. Fromentin G, Poulachon G, Moisan A, et al (2005) Precision and surface integrity of threads obtained by form tapping. CIRP Ann - Manuf Technol 54:519-522.
19. Piska M, Sliwkova P (2015) A study of cutting and forming threads with coated HSS taps. J Mach Eng 15:65-74.
20. Chuan-Chi Hsu, Syh-Shiuh Yeh, Jien-I Lee (2016) Effect analysis and optimal combination of cutting conditions on the cutting torque of tapping processes using Taguchi methods. In: 2016 IEEE International Conference on Automation Science and Engineering (CASE), pp 1215-1218.

21. Bratan S, Novikov P, Roshchupkin S (2016) Application of Combined Taps for Increasing the Shaping Accuracy of the Internal Threads in Aluminium Alloys. Procedia Eng 150:802-808.
22. Ahmadi K, Altintas Y (2013) Stability of lateral, torsional and axial vibrations in drilling. Int J Mach Tools Manuf 68:63-74.
23. Ma YC, Wan M, Yang Y, Zhang WH (2019) Dynamics of tapping process. Int J Mach Tools Manuf 140:34-47.
24. Bayly PV, Young KA, Calvert SG, Halley JE (2001) Analysis of tool oscillation and hole roundness error in a quasi-static model of reaming. J Manuf Sci Eng 123:387-396.
25. Deng CS, Chin JH (2004) Roundness errors in BTA drilling and a model of waviness and lobing caused by resonant forced vibrations of its long drill shaft. J Manuf Sci Eng 126:524-534.
26. Whitehead BT, Bayly PV, Calvert SG (2001) The Effect of Process Damping On Stability and Hole Form in Drilling. SAE International, Warrendale, PA.
27. S Towfighian, K Behdinan, M Papini, et al (2007) Finite element modeling of low speed reaming vibrations with reamer geometry modifications. J Intell Manuf 18:647-661.
28. Chen NM, Smith AJR (2011) Modelling of straight-flute machine tapping. Proc Inst Mech Eng Part B J Eng Manuf 225:1552-1567.
29. Kaymakci M, Kilic ZM, Altintas Y (2012) Unified cutting force model for turning, boring, drilling and milling operations. Int J Mach Tools Manuf 54-55:34-45.
30. Ahmadi K, Savilov A (2015) Modeling the mechanics and dynamics of arbitrary edge drills. Int J Mach Tools Manuf 89:208-220.
31. Jiménez A, Arizmendi M, Cumbicus WE (2018) Model for the prediction of low-frequency lateral vibrations in drilling process with pilot hole. Int J Adv Manuf Technol 96:1971-1990.
32. Eynian M, Altintas Y (2010) Analytical Chatter Stability of Milling With Rotating Cutter Dynamics at Process Damping Speeds. J Manuf Sci Eng 132:021012.
33. Wang C, Guan W, Wang JY, et al (2018) Adaptive operational modal identification for slow linear time-varying structures based on frozen-in coefficient method and limited memory recursive principal component analysis. Mech Syst Signal Process 100:899-925.
34. Insperger T, Stépán G (2011) Semi-Discretization for Time-Delay Systems. Springer New York, New York.

Figures

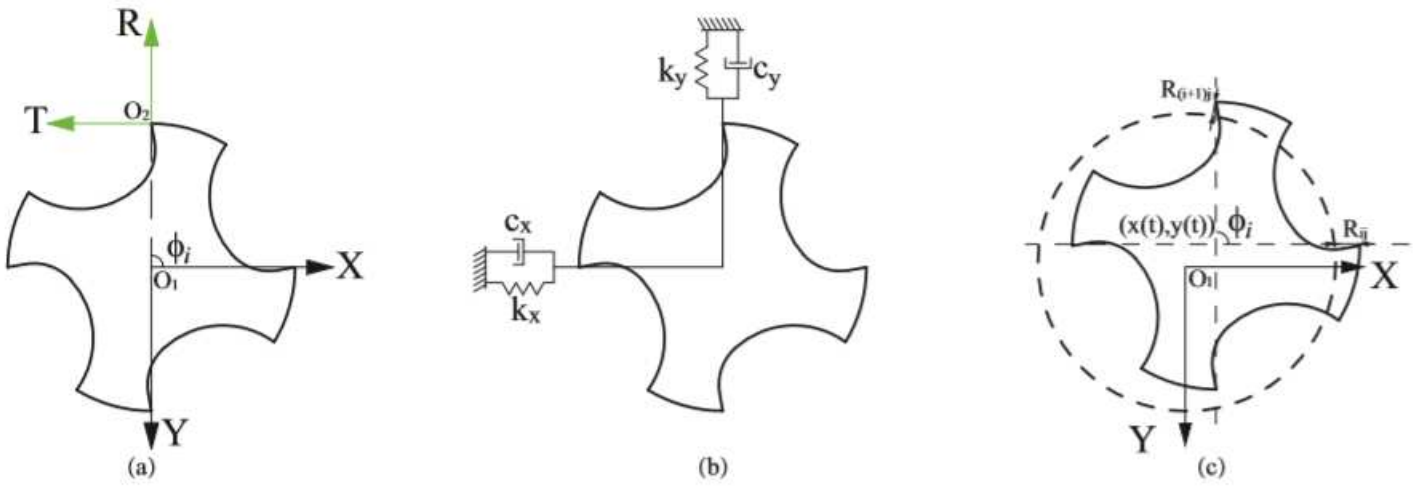

Figure 1

Dynamic model of tapping process by considering the transverse vibrations

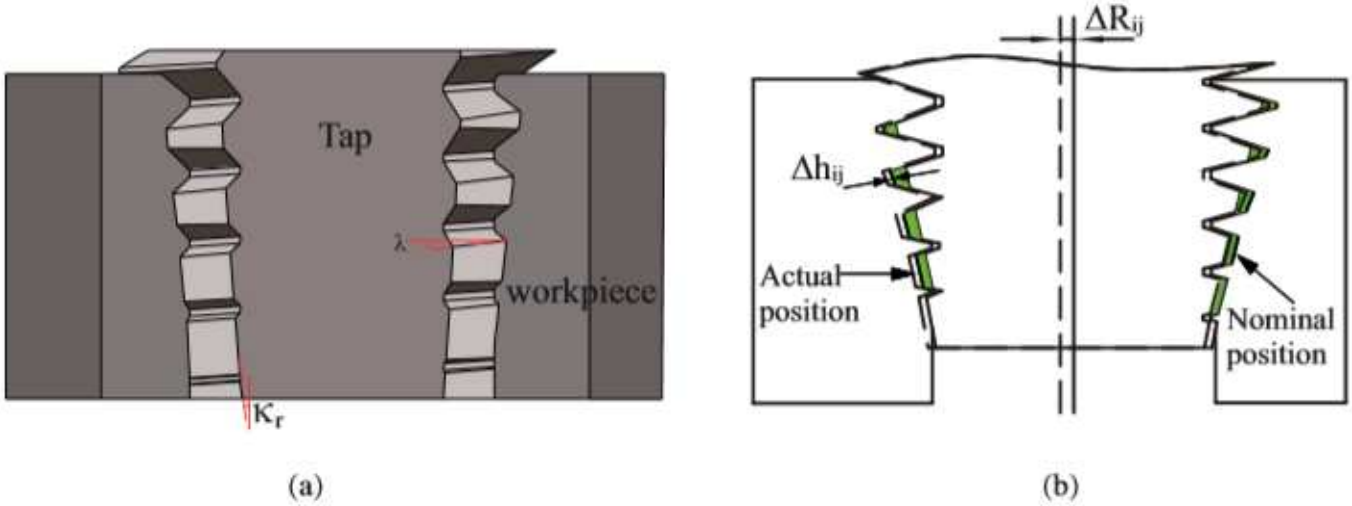

Figure 2

Position change of the tap axis under transverse vibration

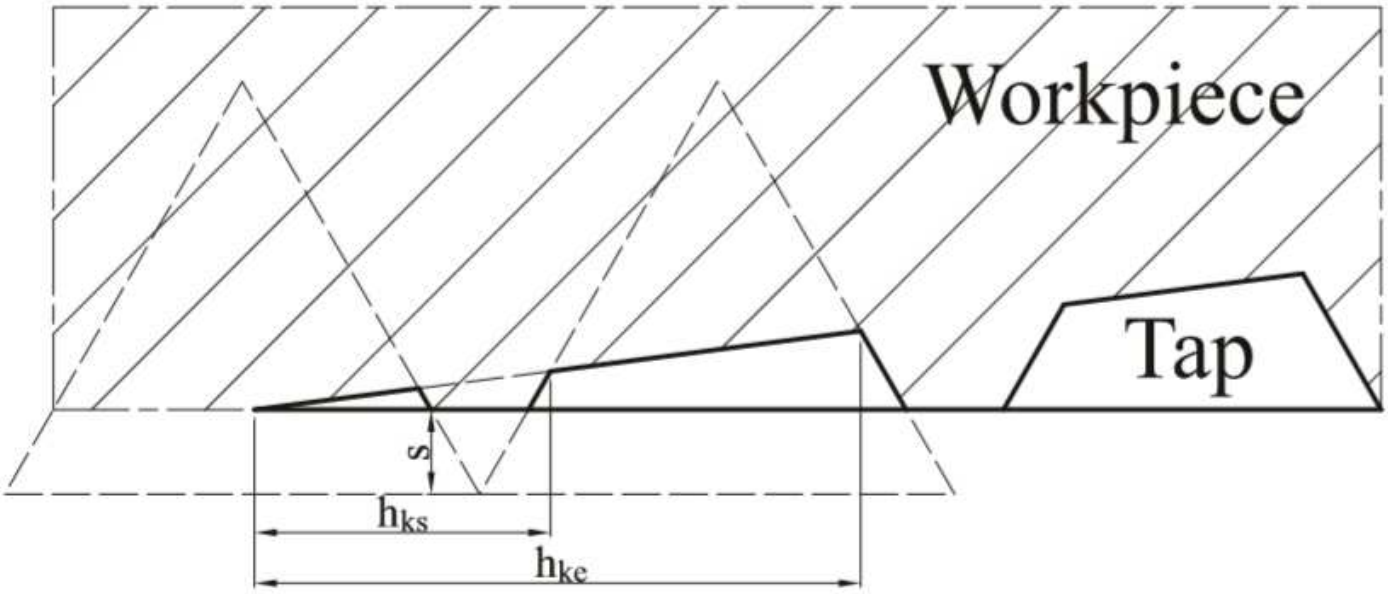

Figure 3

Axial position of each cutting edge on the straight flute tap

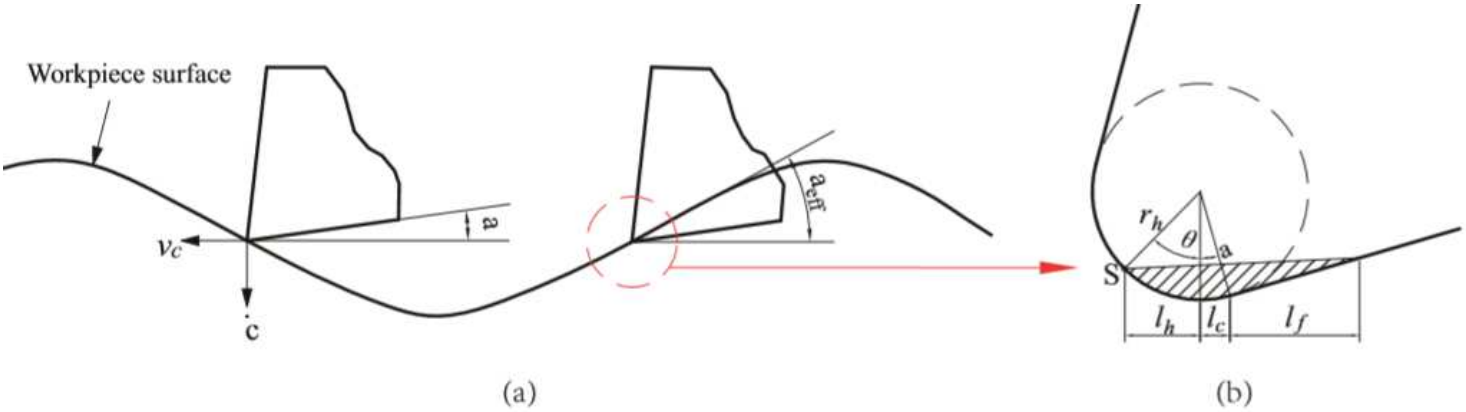

Figure 4

Tool path and cutting damping force geometry

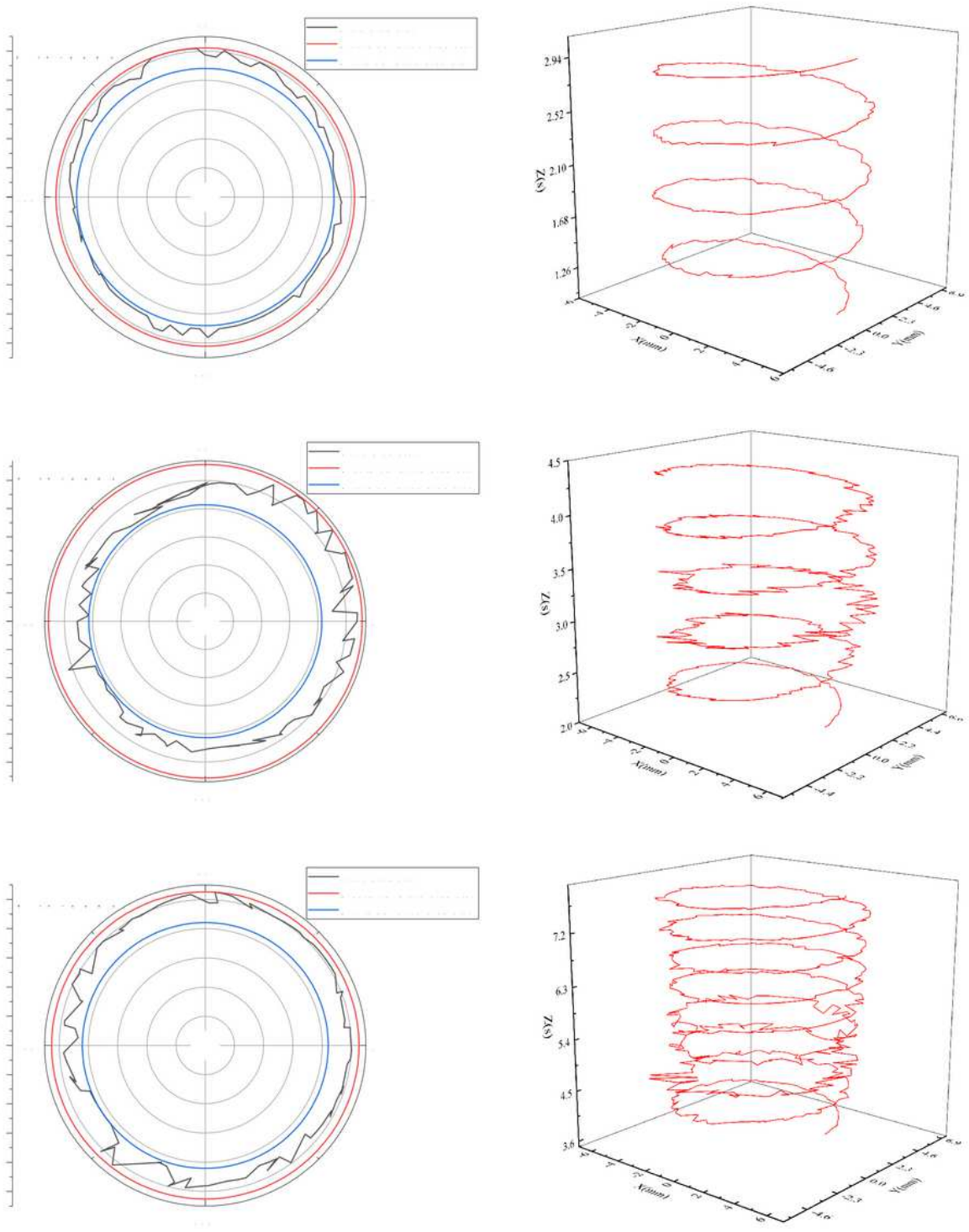

Figure 5

Change of the pitch diameter of the first full thread and the movement trajectory of the outermost cutting edge of the tap in the global coordinate system during the entire cutting process when the chamfer length is 2 threads, 4 threads and 8 threads

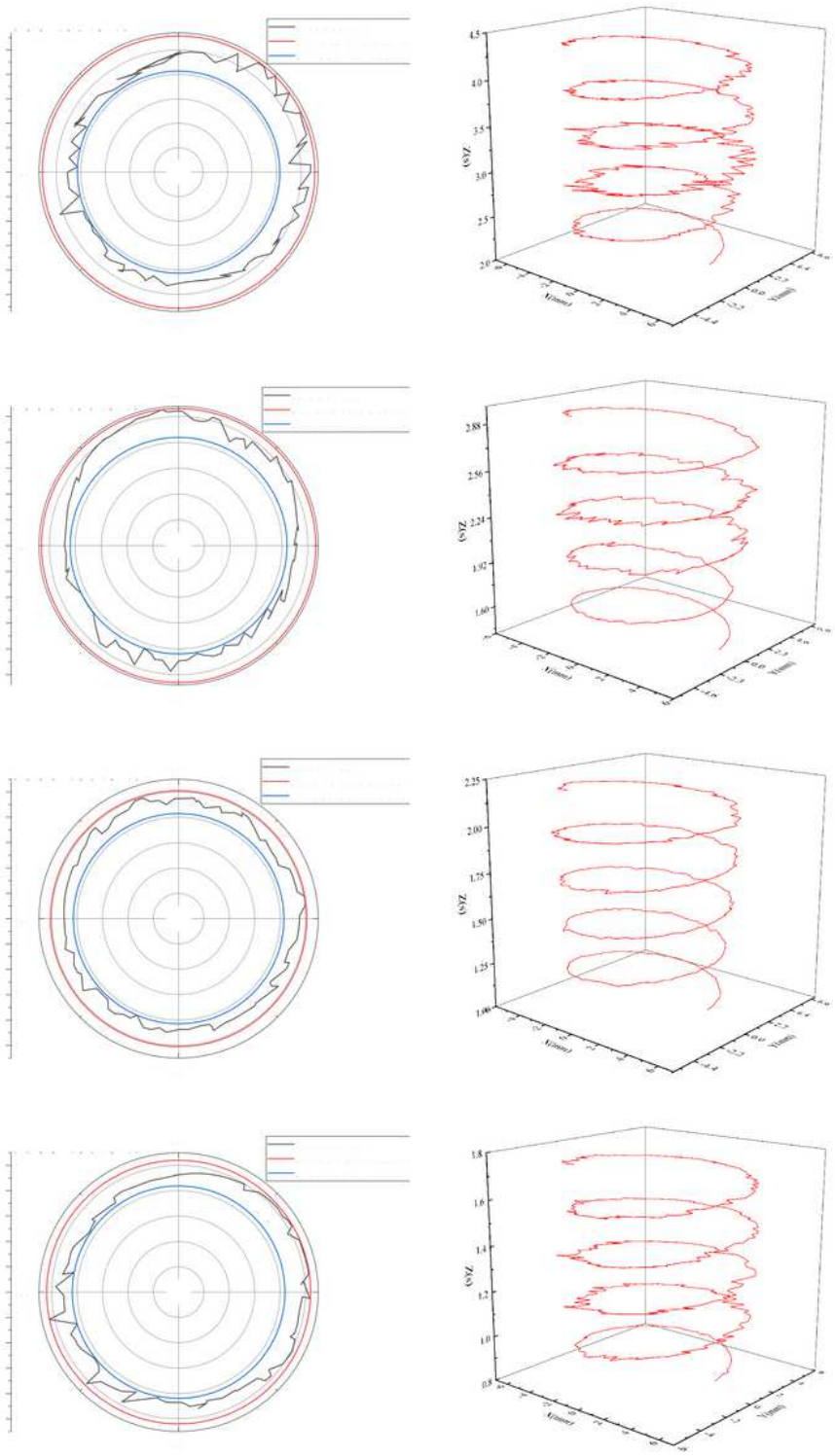

Figure 6

Change of the pitch diameter of the first full thread and the movement trajectory of the outermost cutting edge of the tap in the global coordinate system during the entire cutting process when the spindle speed is 700rev/min, 1050rev/min, 1400rev/min and 1750rev/min

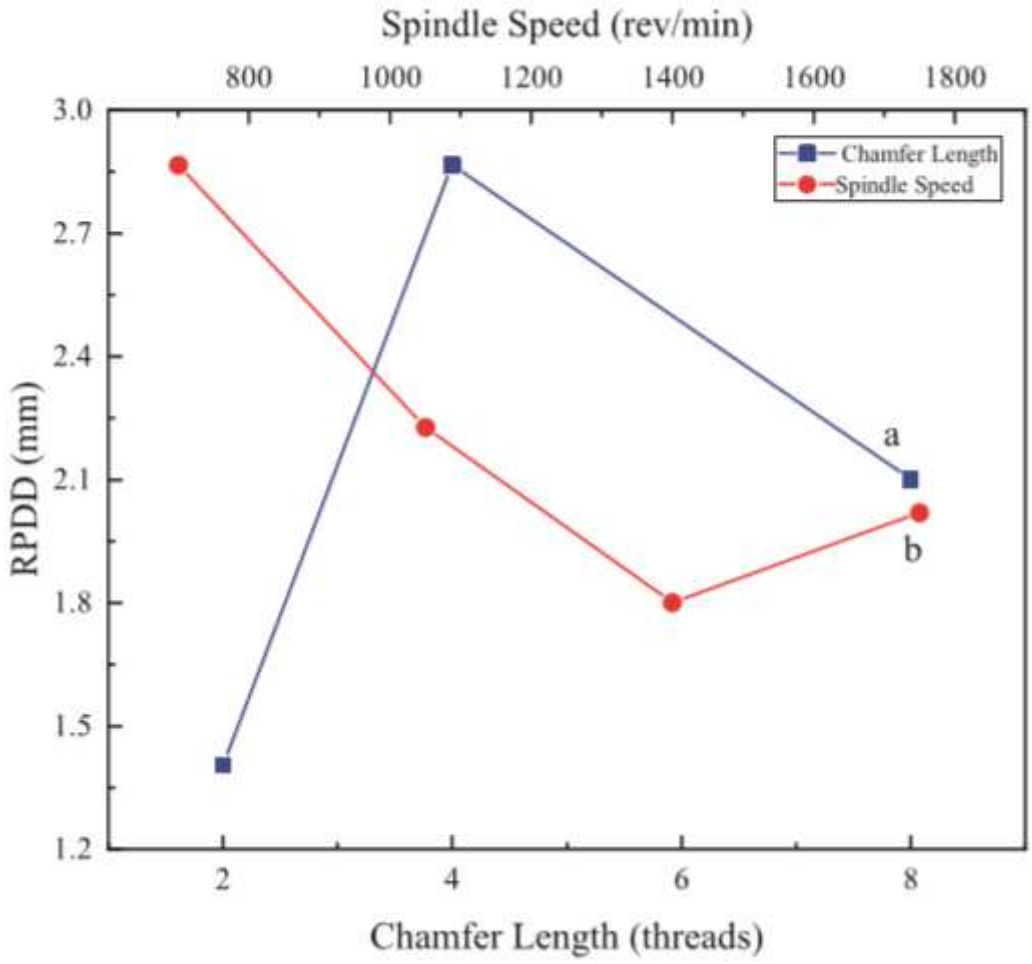

Figure 7

Dimensional of RPDD under different spindle speed and chamfer length